The Journal of Chemical Physics

RESEARCH ARTICLE | JUNE 24 2025

Translational diffusion in supercooled water at and near the glass transition temperature—136 K

Greg A. Kimmel ; Megan K. Dunlap ; Kirill Gurdumov ; R. Scott Smith ; Loni Kringle ; Bruce D. Kay

J. Chem. Phys. 162, 244505 (2025)
https://doi.org/10.1063/5.0264917
CHORUS

The Journal of Chemical Physics ARTICLE pubs.aip.org/aip/jcp

Translational diffusion in supercooled water at and near the glass transition temperature—136 K

Cite as: J. Chem. Phys. 162, 244505 (2025); doi: 10.1063/5.0264917
Submitted: 12 February 2025 • Accepted: 5 May 2025 •
Published Online: 24 June 2025

Greg A. Kimmel,[a] Megan K. Dunlap, Kirill Gurdumov, R. Scott Smith, Loni Kringle, and Bruce D. Kay

AFFILIATIONS

Physical Sciences Division, Pacific Northwest National Laboratory, P.O. Box 999, Richland, Washington 99352, USA

[a]Author to whom correspondence should be addressed: gregory.kimmel@pnnl.gov

ABSTRACT

The properties of amorphous solid water at and near the calorimetric glass transition temperature, T_g, of 136 K have been debated for years. One hypothesis is that water turns into a "true" liquid at T_g (i.e., it becomes ergodic) and exhibits all the characteristics of an ergodic liquid, including translational diffusion. A competing hypothesis is that only rotational motion becomes active at T_g, while the "real" glass transition in water is at a considerably higher temperature. To address this dispute, we have investigated the diffusive mixing in nanoscale water films, with thicknesses up to ~100 nm, using infrared (IR) spectroscopy. The experiments used films that were composed of at least 90% H_2O with D_2O making up the balance and were conducted under conditions where H/D exchange was essentially eliminated. Because the IR spectra of multilayer D_2O films (e.g., thicknesses of ~3–6 nm) embedded within thick H_2O films are distinct from the spectrum of isolated D_2O molecules within H_2O, the diffusive mixing of (initially) isotopically layered water films could be followed as a function of annealing time and temperature. The results show that water films with total thicknesses ranging from ~20 to 100 nm diffusively mixed prior to crystallization for temperatures between 120 and 144 K. The translational diffusion had an Arrhenius temperature dependence with an activation energy of 40.8 ± 3.5 kJ/mol, which indicates that water at and near T_g is a strong liquid. The measured diffusion coefficient at 136 K is $6.25 \pm 1.4 \times 10^{-21}$ m^2/s.

I. INTRODUCTION

At sufficiently low temperatures (e.g., 100 K or less), water can adopt a variety of non-crystalline forms that are unable to relax on an experimentally accessible timescale. In an early report, Burton and Oliver found that depositing water vapor on a cold Cu rod at temperatures around 120 K produced an amorphous solid,[1] which is commonly called amorphous solid water (ASW). In 1985, Mayer showed that crystallization in liquid water could be avoided if micrometer-scale droplets were sprayed onto a cold substrate, producing hyperquenched glassy water (HGW).[2] Alternatively, Mishima and co-workers showed that compressing hexagonal ice, I_h, at 77 K produced amorphous ice,[3] which, upon recovery to ambient pressure, had a density of ~1.17 g/cm^3 and was thus called high density amorphous ice (HDA). Interestingly, upon annealing to ~135 K, HDA converts to a distinct polymorph—low density amorphous ice (LDA). When compressed, LDA reverts to HDA via a first-order-like transition.[4] At low pressures, other amorphous solids, such as very high density and medium density amorphous ices (VHDA and MDA, respectively), have also been identified.[5,6] The properties of amorphous solids at high pressures are also of great interest.

The possible connections between ASW, HGW, and LDA have been extensively investigated.[7–9] One key question is as follows: What happens to these amorphous solids as the temperature is increased to the point where the structure is no longer kinetically arrested?[9] One hypothesis is that they turn into the same supercooled liquid at 136 K, such that they exhibit all the properties characteristic of normal liquids, including rotational and translational diffusion, D_{rot} and D_{tr}, respectively. (Below, we will refer to

the translational diffusion of water molecules as simply "diffusion.") Using differential scanning calorimetry (DSC), a weak endotherm, which is found at ~136 K for LDA, ASW, and HGW, has been identified as the onset of liquid-like behavior. In that case, the corresponding glass transition temperature, T_g, would be 136 K.[10,11] A second hypothesis is that this weak endotherm is associated with the unfreezing of rotational motion, but not diffusion, in these amorphous solids and that the true glass–liquid transition occurs at much higher temperatures (e.g., ~165 K).[12,13] Yet, a third hypothesis is that the amorphous ices are unstable with respect to crystalline ice, and any observed changes are the result of an amorphous-to-crystalline transition. These and other hypotheses are discussed in detail in several excellent reviews.[7–9]

One of the primary motivations for developing a detailed understanding of how amorphous ices transform when they are warmed up relates to persistent questions about the structure and dynamics of normal and supercooled liquid water and its many anomalous properties.[7,14–16] A leading hypothesis proposes that liquid water at low temperatures and high pressures can exist in two distinct forms—a high-density liquid (HDL) and a low-density liquid (LDL)—that are separated by a two-phase coexistence line that terminates in a second critical point. One appealing aspect of this liquid–liquid critical point (LLCP) hypothesis is that it provides a natural explanation for HDA and LDA. Namely, they are the glassy analogs of HDL and LDL.[7] Because a second critical point—if it exists—will be at high pressure, experiments at and near ambient pressures cannot probe it directly. However, the LLCP hypothesis and several related theories predict that LDA should be connected to water at ambient conditions by a thermodynamically reversible path.[7,14–19] While several recent experiments support this picture,[20–23] they have not addressed whether LDA turns into a "true" liquid at/near the glass transition temperature before it eventually crystallizes. Therefore, experiments that address this issue will provide valuable information about the feasibility of the LLCP and other hypotheses for water's unusual behavior.

Angell noted that "the most fundamental of the transport properties is the self-diffusion coefficient since no external stress is required to manifest, or measure, the property."[24] The question of whether diffusion occurs in ASW, HGW, and LDA has been controversial since at least 1995 when Fisher and Devlin investigated H/D exchange in amorphous H_2O films that had been doped with a low concentration of isolated D_2O.[12] Protons were injected into the films through photoexcitation of 2-napthol, and the H/D exchange kinetics, which first converted isolated D_2O to 2 adjacent HOD ("coupled HOD") and then to isolated HOD, were monitored via infrared spectroscopy. Fisher and Devlin argued that the observed kinetics ruled out diffusion in ASW and instead suggested that molecular rotations were sufficient to explain their results. Subsequently, Johari challenged Fisher and Devlin's interpretation noting that diffusion could also account for the observations.[25] Recently, elegant experiments from Shephard and Salzmann have examined the influence of isotopes (H_2O, $H_2{}^{18}O$, and D_2O) on the calorimetric glass transition temperatures in LDA, HDA, and crystalline ice VI.[13] As they noted, hydrogen-disordered ice VI is an interesting case because its glass transition is due to unfreezing of molecular rotations—no diffusion is involved. Using DSC, they found that (i) the magnitude of endotherms for LDA and ice VI was comparable, (ii) their T_g's were nearly the same, and (iii) the transition temperatures showed essentially identical isotopic shifts. Based on the similarities between LDA and ice VI, they concluded that the experimentally observed glass transition in LDA (and also HDA) involves only rotational motion. More recently, Melillo *et al.* have investigated the glass transition in confined water using calorimetry and dielectric spectroscopy.[26] They found that T_g occurred at temperatures between ~170 and 200 K (depending on the system). Comparing the small heat capacity changes observed in confinement and in bulk LDA at ~136 K, they concluded that the bulk T_g must be at significantly higher temperatures.

Vapor deposition onto cold surfaces in ultrahigh vacuum with various isotopologues of water allows one to create isotopically layered amorphous solid water films.[27] Upon heating, such layered films have been used to investigate dynamic processes, including mixing within nanoscale water films.[28–30] For example, the mixing within layered $H_2{}^{18}O/H_2{}^{16}O$ films, which was monitored via desorption into the gas phase, occurred in concert with crystallization of the films at ~155 K.[29,30] A model that treated the crystallization kinetics and assumed diffusion within in the liquid portion of the crystallizing films (with negligible diffusion in the crystalline portion) was able to reproduce the observations. However, subsequent experiments showed that the crystallization heavily influenced the mixing process, precluding an accurate determination of the diffusion in the liquid portion from those measurments.[31,32]

Fluidity—which is connected to diffusion—is one of the hallmarks of liquids. In a recent review of "Water's controversial glass transitions," Amann-Winkel *et al.* noted that "the key question, to us, remains whether above the glass transition the water molecules display liquid-like bulk fluidity or not."[9] However, many of the experimental approaches used to date do not directly address this issue or had various experimental limitations. Those authors suggest that detailed measurements of the shear viscosity are one approach to this problem, while "diffusion measurements probing the transport of *oxygen* [emphasis in the original] will do the job."

Here, building upon recent experiments showing that H/D exchange can be effectively eliminated in nanoscale water films,[33] we use infrared spectroscopy to investigate the diffusive mixing of (intact) D_2O molecules in H_2O films at and below the traditional glass transition temperature (T_g = 136 K). The results demonstrate long range translational diffusion (e.g., >5 nm) of molecular D_2O in water at temperatures from 120 to 144 K. The diffusive mixing of the films is independent of the total film thicknesses, x_{film}, in the range of ~20–100 nm. Within the uncertainty of our experiments, we find that the measured diffusion is not influenced by the water/substrate or water/vacuum interfaces and is instead characteristic of the bulk liquid. The diffusion is activated with simple Arrhenius temperature dependence and an activation energy, E_a, of 40.8 ± 3.5 kJ/mol. The results indicate that water at and near the glass transition is a strong, supercooled liquid. Furthermore, the Wilson–Frenkel model[34–36]—which posits that the growth rate of a crystalline phase in contact with its melt is proportional to the diffusion coefficient within the liquid—holds for supercooled water near T_g.

II. EXPERIMENTAL METHODS

The experiments were performed in an ultrahigh vacuum (UHV) system, which had typical base pressures of 1.3×10^{-8} Pa

or less, that has been described in detail previously.[37] For the results reported here, the relevant components were a closed-cycle helium cryostat (Advanced Research Systems, CSW-204B), an effusive molecular beam dosing line, a quadrupole mass spectrometer (Extrel, Merlin), and a Fourier transform infrared spectrometer (Bruker, Vertex 70). The cryostat allowed a Pt(111) single crystal (1 cm diameter, 2 mm thick) to be cooled to a base temperature of ~25 K. Heating and isothermal temperature control were achieved by resistively heating thin tantalum wires spot-welded to the back of the crystal. The temperature was monitored with a K-type thermocouple, also spot-welded to the back of the crystal. Because the experiments reported below were conducted at constant temperature and the potential sources of heat loss or gain (e.g., due to water desorption or absorption of black body radiation from the vacuum chamber walls, respectively) were small, we estimate that any resulting temperature gradients, ΔT_{film}, across the water films (i.e., perpendicular to the Pt(111) surface) were less than 1 mK.

The Pt(111) crystal was cleaned by sputtering with 2 keV Ne^+ and then annealing at 1000 K in vacuum. Nanoscale films of H_2O and D_2O were adsorbed onto the crystal at normal incidence at 108 K using the molecular beam with fluxes of ~2×10^{18} m^{-2} s^{-1}. These conditions produced a non-porous, amorphous solid water (ASW) film.[38,39] For temperatures below ~115 K, diffusion is negligible on the timescale for depositing the water films, and the results reported below are independent of the deposition temperature for (at least) 80 K $\leq T \leq$ 115 K. The central portion of the molecular beam (the umbra) had a diameter of 8.5 mm, while at the edge of the crystal, the flux decreased by ~20% (i.e., in the penumbra). Water coverages, θ, are given in units of water monolayers (MLs) on Pt(111), which were determined using temperature programmed desorption (TPD). For a water "monolayer" on Pt(111), there are two closely related structures corresponding to a single monolayer on Pt(111), the $\left(\sqrt{37} \times \sqrt{37}\right)$R25.3° structure and the $\left(\sqrt{39} \times \sqrt{39}\right)$R16.3° structure.[40] They have coverages of 1.054 and 1.077×10^{15} molecules/cm^2, respectively, and are difficult to distinguish in the TPD spectra, but this uncertainty is small compared to other sources of error in the measurements. Below, some results are discussed in terms of the thickness of various water layers. To convert water coverages to thicknesses, we assumed 1 ML = 0.33 nm. (For LDA at 80 K, the density is 937 kg/m^3,[41] and the typical distance between molecules r_{nn} can be estimated as $r_{nn} \sim N^{-1/3} \sim 0.32$ nm, where N is the number density.)

Water films with a total coverage, θ_{total}, of 200 ML, corresponding to a thickness of ~66 nm, were used for most of the experiments presented below. However, as shown in Secs. III and IV, the same behavior was found for films with coverages from 60 to 300 ML, corresponding to thicknesses of ~20–100 nm. Furthermore, in most of the experiments, the D_2O layers were sufficiently far from the water/Pt and water/vacuum interfaces that processes occurring at those interfaces did not influence the results. The disruption of the bulk hydrogen-bonding network in the vicinity of these interfaces could alter the structure and dynamics there, making them unrepresentative of the bulk transport properties. For example, crystallization in nanoscale water films occurs preferentially at the vacuum interface, presumably due to the enhanced mobility and excess free volume for water molecules there.[42] In another example, the enhanced mobility of molecules at the vacuum interface can lead to the formation of exceptionally stable glasses during vapor deposition.[43,44]

To investigate molecular diffusion using layered films of D_2O and H_2O, it was necessary to suppress H/D exchange. As mentioned already in the Introduction, H/D exchange can convert D_2O into HOD. In that case, repeated H/D exchange reactions combined with molecular rotations can lead to transport of hydrogenic mass over appreciable distances, even in the absence of molecular diffusion.[12] Because the relative rates for molecular rotations and diffusion are not known near T_g, experiments with appreciable H/D exchange do not provide an unambiguous method for measuring diffusion.[9] However, at temperatures near T_g, autoionization in water is very low, and recent work in our group has shown that H/D exchange can be suppressed if exogenous sources of excess protons are removed.[33] The primary source of protons for the experiments reported here was from dissociative adsorption of H_2 on the Pt(111) substrate that occurred as the sample cooled after rapid heating to high temperatures. (The "flash" heating was performed to remove any volatile species from the surface prior to adsorbing the water films. H_2 is typically one of the primary residual gases in ultrahigh vacuum systems.) Once water was deposited and the system was heated, the adsorbed H atoms reacted with the water to form hydrated protons that subsequently diffuse into the film, leading to H/D exchange between D_2O and H_2O. However, this problem was avoided by adsorbing small amounts of O_2 on the surface prior to adding the water. The oxygen effectively scavenged the adsorbed H, suppressing the H/D exchange but not eliminating it entirely.[33] However, any remaining excess protons established a distance-dependent distribution within the film, such that they were primarily localized near the Pt substrate.[37] Because the infrared (IR) signal for isolated D_2O is easily distinguished from the signal for isolated HOD,[12,37] it was relatively straightforward to monitor the production of isolated HOD (if any) during the course of the experiments. For example, in some experiments where the evolution of the water films was monitored for long times, D_2O diffused into the vicinity of the Pt substrate and some H/D exchange occurred.

Water films in UHV systems are metastable with respect to both crystallization and desorption (sublimation/vaporization). The experiments reported below were designed to probe processes in water films at/near T_g that were not affected by crystallization or desorption. In IRAS, crystallization can typically be detected once the crystalline fraction has reached ~0.01–0.02.[22,45] The results presented below focus on times prior to the onset of crystallization. For T < 136.5 K, no crystallization was detected during the experiments. However, for some experiments at higher temperatures, the films eventually crystallized at longer times. In those cases, only data prior to detectable crystallization were included in the analysis. Furthermore, the times most relevant for analyzing the diffusion were considerably less than the crystallization time. For example, the onset of crystallization was observed at ~2700 s for a film annealed at 140 K. Below, we will show that a typical water molecule would have diffused x_{diff} ~16 nm during that time [where $x_{diff} \sim \sqrt{6D_{tr}t}$ (in 3 dimensions)]. The experiments started with D_2O films, θ_{D_2O} = 2–20 ML, (i.e., ~0.66–6.6 nm) deposited at various locations within H_2O films (e.g., Fig. 1(a)). Desorption from the water films did not appreciably affect the results for experiments where the coverage of an H_2O cap layer, θ_{cap}, deposited on top of the D_2O layer

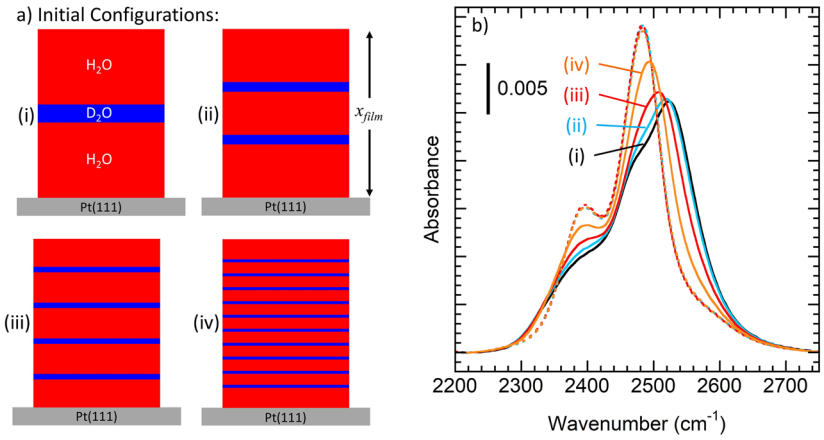

FIG. 1. (a) Schematic of the initial sample configurations. All the films comprised 180 ML H_2O and 20 ML D_2O arranged in four different configurations: (i) A single 20 ML D_2O layer embedded in the middle of the H_2O, (ii) 2 × 10 ML D_2O layers, (iii) 4 × 5 ML D_2O layers, and (iv) 10 × 2 ML D_2O layers. (b) IRAS spectra for the 4 water films with different initial configurations. The spectra before annealing (solid lines) are all distinct, while those after annealing (dotted lines) are essentially identical. The IR spectra before (during) annealing were taken at 108 K (134.5 K). The annealing times for the 4 films were (i) 2.1 × 10^4 s, (ii) 5270 s, (iii) 1330 s, and (iv) 209 s.

was large compared to amount that desorbed during the experiment. Those experiments included films with θ_{total} = 200 ML, a 20 ML D_2O layer, and θ_{cap} = 90 ML. For experiments with D_2O layers at or near the vacuum interface, desorption did not qualitatively change the results. However, to obtain quantitative results, desorption was included in the analysis.

In the results presented below, the OD-stretch region (~2200–2750 cm^{-1}) of the IRAS spectra was analyzed to assess the diffusive mixing in D_2O/H_2O water films. In this wavenumber range, H_2O has a broad "association band," attributed to the H_2O bending mode plus librations,[46,47] that overlaps with the OD-stretching region (see Fig. S1). The contribution of this H_2O band has been subtracted prior to analysis and displaying the spectra.

To model diffusion in the water films, the one-dimensional diffusion equation was solved by converting it into a series of coupled ordinary differential equations (representing the layers within the films). The initial conditions were chosen to match the experimental configurations in the layered films of H_2O and D_2O [e.g., Fig. 1(a)]. A reflecting boundary condition was imposed at the water/Pt and water/vacuum interfaces. For some experiments, D_2O layers were deposited at or near the vacuum interface. As noted above, desorption was not negligible for those experiments, and it was included in the calculations. Although the desorption rate for films of pure D_2O and H_2O is different at a given temperature, the D_2O and H_2O were assumed to desorb at the same rate in the simulations. Test calculations, which varied the desorption rate, indicated that this did not appreciably influence the results.

III. RESULTS

To address molecular translational diffusion in "bulk" water, the experiments used infrared reflection absorption spectroscopy (IRAS) to monitor the evolution vs time in the OD-stretching region of water films that were deposited with layers of D_2O embedded within H_2O in various configurations [e.g., Fig. 1(a)]. The water layers were grown under conditions where diffusion was negligible and the initial concentration of D_2O in the film was zero except in well-defined layers. If molecular diffusion is appreciable, then upon annealing to higher temperature, the overall concentration of D_2O will evolve toward a constant determined by the relative amounts of H_2O and D_2O within the film. IRAS can monitor this process because IR spectra in the OH- and OD-stretching regions are sensitive to the local hydrogen bonding arrangement.[48] Here, we use the fact that D_2O molecules isolated within an H_2O matrix have an IR spectrum in the OD-stretch region (~2200–2750 cm^{-1}) that is distinct from those of both pure D_2O and isolated HOD (see Fig. S2).[12,37] For the results presented below, the IR spectra of the as-deposited films were taken at 108 K, and all the subsequent spectra were taken at the annealing temperature for any given experiment (unless otherwise noted).

Figure 1(b) shows several spectra for water films that had θ_{total} = 200 ML (i.e., x_{film} ~ 66 nm), with θ_{H_2O} = 180 ML and θ_{D2O} = 20 ML. While the films all contained 20 ML D_2O, the initial spatial arrangement of the D_2O was different in each film [Fig. 1(a)]. As a result, the IR spectra before annealing were all distinct [Fig. 1(b), solid lines]. The IR spectra of films grown with fewer, but thicker, D_2O layers more closely resemble the spectra of "bulk" D_2O because they have fewer D_2O molecules influenced by nearby H_2O (see Fig. S2). In contrast, after annealing for various times at 134.5 K, all the films evolved to the point where they had a nearly identical spectrum that was dominated by two distinct peaks at 2478 ± 2 and 2392 ± 2 cm^{-1} [Fig. 1(b), dotted lines]. IR spectra were also obtained for films with lower D_2O concentrations dispersed in H_2O (see Fig. S3), and they were similar to the final spectra shown in Fig. 1. The IR spectra observed after sufficient annealing are characteristic of isolated D_2O and are quite similar to previous reports.[12,33,37,49] The peaks at 2478 and 2392 cm^{-1} correspond to the asymmetric and symmetric stretch, respectively, of D_2O.[49] The lack of HOD in the IR spectra after annealing shows that H/D exchange has been effectively suppressed in these experiments. The lack of an IR peak

associated with the HOD bending mode provides further evidence of this (see Fig. S4). Note that as the thickness of the individual D_2O layers increased in Fig. 1, the annealing time required for the resulting IR spectra to resemble isolated D_2O increased rapidly. For film (i), which had a single 20 ML D_2O layer, to sufficiently mix to have a similar spectrum to the other starting configurations suggests that water molecules within that film diffused distances that were on the order of 10 nm.

For the experiments shown in Fig. 1, 10% of the water molecules were D_2O, while the remaining 90% were H_2O. At this concentration, if all the water molecules form 4 hydrogen bonds and are randomly distributed with respect to the isotopologues, then 66% of the D_2O will have 4 H_2O neighbors and another 29% will have only 1 D_2O neighbor. As a result, isolated D_2O and D_2O "dimers" will account for 95% of the total D_2O in the water film. Here, we refer to low concentrations of D_2O dispersed in H_2O as "isolated D_2O," but it is useful to remember that the actual amount of D_2O nearest neighbors (or other D_2O clusters) is a sensitive function of the local concentration.

For experiments with a single multilayer D_2O slab in the middle of an H_2O film [see Fig. 1(a-i)], the IR spectra showed a characteristic evolution vs time when the films were annealed at temperatures where diffusion was appreciable. For example, Fig. 2(a) shows a series of IR spectra in the OD-stretch region for a film with one 20 ML D_2O layer in the middle of 180 ML H_2O. Before annealing, the peak in the spectrum was at ~2490 cm^{-1} [Fig. 2(a), black line]. Upon annealing at 132.5 K, the peak continuously shifted to lower wavenumbers [Fig. 2(a), red lines]. At the same time, an initial shoulder at ~2395 cm^{-1} developed into a distinct peak at later times. The changes in the IR spectra upon annealing can be highlighted by taking the difference between the spectra at any given time and the first spectrum at T_{anneal} [Fig. 2(b)]. The difference spectra emphasize the emergence of the two lower frequency peaks in the IR spectra at later times.

For water, the IR spectra in the OH- and OD-stretch regions are very sensitive to the local environment,[48] including the local concentration of H_2O and D_2O. They also reflect the sum of the contributions from all the molecules. For experiments such as those shown in Figs. 1 and 2, the D_2O molecules experience a time-dependent range of local concentrations, which makes it difficult to extract the self-diffusion coefficient for water directly from the observed IR spectra. However, for films with 20 ML D_2O in the middle of 180 ML H_2O that were subsequently annealed at different temperatures, the IR spectra evolved through essentially the same sequence as shown in Fig. 2, but the amount of time needed to progress through the sequence depended on the temperature. Qualitatively, this is just what one expects for a system that diffusively mixes from an initially layered configuration. In that case, there is a characteristic time at each temperature, $\tau(T)$ that is proportional to $\lambda^2/D_{tr}(T)$, where λ is a characteristic length within each film. For films with the same initial configuration, λ does not depend on temperature, so the time dependence observed in the experiments is related to $D_{tr}(T)$. While it is difficult to determine $D_{tr}(T)$ directly from the IR spectra, we demonstrate next that it is straightforward to determine $\tau(T)$ (e.g., Fig. 3). Another set of experiments (discussed below) then allow us to relate $\tau(T)$ to $D_{tr}(T)$.

To assess the timescales for the changes in the IR spectra due to diffusive mixing of the water layers at various temperatures,

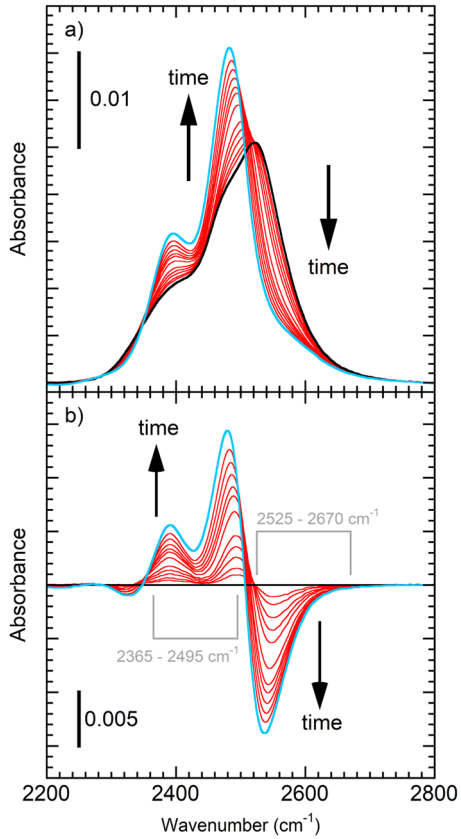

FIG. 2. (a) IR spectra in the OD-stretch region for a film that started with 20 ML D_2O deposited in the middle of 180 ML H_2O [see Fig. 1(a-i)]. All the spectra were acquired at 132.5 K during annealing. The first spectrum at 132.5 K (black line) is similar to the as-deposited spectrum acquired at 108 K (not shown). The spectrum after annealing for 4.4×10^4 s (blue line) is characteristic of isolated D_2O in H_2O. The intermediate spectra (red lines) were taken at 82, 164, 370, 660, 1080, 2650, 4510, 6020, 9040, and 1.38×10^4 s. (b) Difference spectra, where the first spectrum [panel (a), black line] has been subtracted from all the subsequent spectra. With increasing annealing time (red lines), the spectra lose intensity at higher wavenumbers (e.g., 2525–2670 cm^{-1}) and gain intensity at lower wavenumbers (e.g., 2365–2495 cm^{-1}). Figure S1 shows the corresponding raw spectra.

we can track integrals over various portions of the IR bands vs time. Figure 3(a) shows two of these integrals for several temperatures: one on the high-frequency side of the OD-stretch band [2525–2670 cm^{-1}, see Fig. 2(b)] that decreases with time and a second integral on the low-frequency side [2365–2495 cm^{-1}, see Fig. 2(b)] that increases with time. As seen in Fig. 3(a), the time at which a given value of either integral is reached increases substantially at lower temperatures. However, when the times are scaled by $\tau(T)$, the data collapse onto two curves—one for each of the integrals [Fig. 3(b)]. An important observation is that $\tau(T)$ increased exponentially vs $1/T$ with E_a = 40.8 ± 3.5 kJ/mol (see Fig. S6 and Table S1). Figure S5 shows the integrals vs time for all the temperatures, and Sec. S1 of the supplementary material discusses the scaling behavior expected for diffusively mixed films and our method for determining $\tau(T)$.

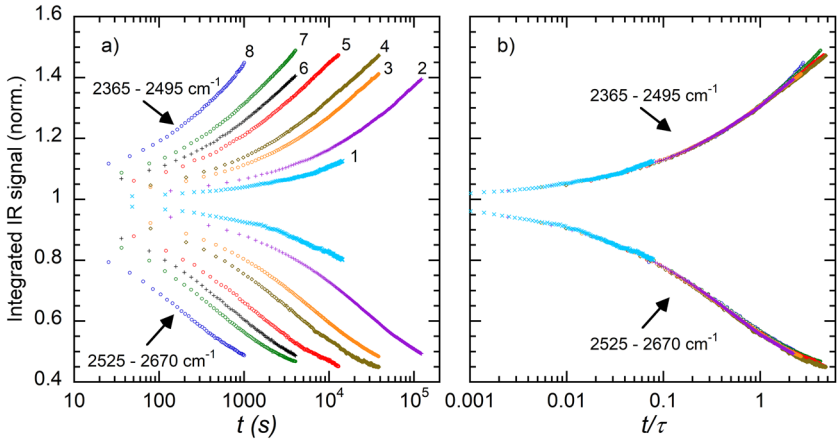

FIG. 3. (a) Integrals over low wavenumber (2365–2495 cm^{-1}) and high wavenumber (2525–2670 cm^{-1}) regions of the OD-stretch band vs time. Water films with one 20 ML D_2O layer in the middle of 180 ML H_2O were annealed at (1) 120.2 K, (2) 124.5 K, (3) 128.5 K, (4) 130 K, (5) 134 K, (6) 136 K, (7) 138.5 K, and (8) 142.5 K. Each symbol in the figure corresponds to an IR spectrum taken at the indicated time and temperature. The increasing signal in the low wavenumber portion of the band is associated with increasingly isolated D_2O, while the decreasing signal at higher wavenumbers is due to the loss of "bulk-like" D_2O. (b) When the times in (a) are scaled by $\tau(T)$, all the data collapse onto two curves, as expected for diffusion. (Fig. S8 displays these data on a linear time scale.)

Qualitatively similar results to those shown in Fig. 3 were obtained for different choices of the integration limits within the increasing or decreasing portions of the IR band. As noted already, this behavior is consistent with diffusive mixing in the films where only the rate of mixing—not the sequence of concentration profiles—depends on the temperature. Similar scaling behavior was also observed for other film geometries (see Fig. S7). For the results shown in Fig. 3, the IR spectra continued to evolve even at the longest times in part because the D_2O was still not uniformly distributed within the water films. While the D_2O should continue to disperse at longer times, several factors worked against conducting longer experiments, including desorption and crystallization of the water films, and an increase in the H/D exchange when D_2O diffused into the vicinity of the platinum substrate (see the discussion in Sec. II). Figure S9 shows examples for films annealed at higher temperatures that eventually begin to crystallize.

One concern that has been raised with respect to experiments on nanoscale water films is that they might not represent the behavior of bulk liquid water. While numerous classical and *ab initio* molecular dynamics simulations have suggested that the structure and dynamics of water converge to bulk behavior in very short distances (typically less than 3 nm) from water/solid, water/vacuum, or water/air interfaces,[50–52] it is important to investigate if this also holds for water films near T_g. To test this, diffusive mixing was measured in a series of water films with a 10 ML D_2O layer deposited between H_2O cap and spacer layers of increasing thickness separating the D_2O from the interfaces [i.e., similar to Fig. 1(a-i)]. In particular, the as-deposited film structures were $Pt/\theta_{spacer}/10$ ML D_2O/θ_{cap}, where 10 ML $\leq \theta_{spacer} = \theta_{cap} \leq 150$ ML. The corresponding thicknesses for these films were ~10 nm $\leq x_{film} \leq$ 100 nm. For these experiments, if the diffusion was independent of the film thickness, then the concentration vs time would be the same for all the different geometries until D_2O diffused to the water/Pt and water/vacuum interfaces. For water films annealed at 134 K for 8000 s, the IR spectra were essentially identical for H_2O layers ≥45 ML (see Fig. S10). For thinner H_2O cap and spacer layers, the IR spectra begin to show differences at early times because D_2O reached the interfaces sooner. Based on these results, the diffusion coefficient in the nanoscale water films was independent of thickness for at least $x_{film} > 20$ nm.

While it was difficult to determine $D_{tr}(T)$ when the D_2O layers were embedded in the middle of thick H_2O films, it could be measured with experiments for which D_2O layers were deposited at or near the vacuum interface. Figure 4(a) shows IR spectra for an experiment where a 20 ML D_2O layer was adsorbed on top of a 180 ML H_2O film and then annealed at 132.5 K. Initially (black line), the spectrum had a weak, narrow peak at 2727 cm^{-1} due to non-hydrogen bonded OD groups ("dangling ODs") of D_2O molecules at the vacuum interface.[53,54] At later times, D_2O diffused into the H_2O layer such that the total concentration of D_2O at the vacuum interface decreased. As a result, the dangling OD signal gradually decreased [Fig. 4(a), red and blue lines]. As the dangling OD signal decreased, the main OD-stretch band also evolved toward the spectrum characteristic of isolated D_2O in H_2O. We assume that the dangling OD signal was proportional to the fraction of D_2O in the layer at the vacuum interface. In that case, the signal, normalized by its value when the water at the interface was entirely D_2O, gave the relative concentration of D_2O at the interface. Figure 4(b) (symbols) shows the normalized integrated intensity for the dangling OD signal vs time for films annealed at 128.5–138 K. The solid lines show corresponding calculations of the concentration of D_2O at the vacuum interface for diffusion coefficients that range from 7.7×10^{-22} to 1.1×10^{-20} m^2/s. Because desorption from the films was appreciable on the timescale of the experiments, it was also included in the simulation. For example, ~6 ML D_2O and 9 ML H_2O desorbed during the experiment at 138 K [Fig. 4(b), blue circles]. Figure S11(a) shows the data in Fig. 4(b), along with several more experiments at

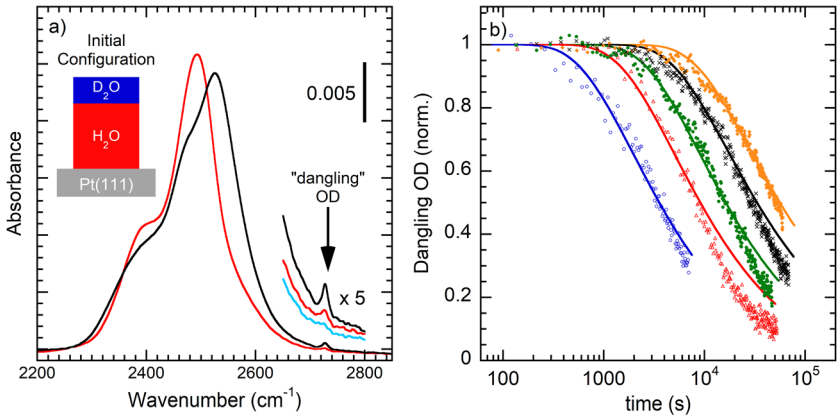

FIG. 4. (a) IR spectra for a 20 ML D_2O film deposited on top of 180 ML H_2O and annealed at 132.5 K. As deposited, the spectrum has a small peak at 2727 cm^{-1} that is due to non-hydrogen-bonded OD groups at the water/vacuum interface (black line). After annealing for 1.9×10^4 s, the OD-stretch band evolves toward a shape characteristic of isolated D_2O, and the intensity of the dangling OD-peak decreases (red line). At even longer times, the dangling OD signal continues to decrease (e.g., 3.9×10^4 s, blue line). The initial spectrum (black line) was taken at 108 K, and the other 2 were taken at 132.5 K. (b) Integrated intensity of the dangling OD peak (symbols) vs time for films annealed at 128.5 (orange diamonds), 130.5 (black crosses), 132.5 (green circles), 134 (red triangles), and 138 K (blue circles). The corresponding IR spectra were taken at the respective annealing temperatures. The solid lines show the surface concentration calculated for diffusion coefficients of 7.7×10^{-22} (orange), 1.3×10^{-21} (black), 2.3×10^{-21} (green), 4.3×10^{-21} (red), and 1.1×10^{-20} m^2/s (blue).

other temperatures. All the results collapse onto a common curve when the times are scaled by $\tau(T)$ [Fig. S11(b)].

A separate set of experiments, which tracked the evolution of the dangling OD signal vs time at 138 K for a D_2O layer deposited at or near the vacuum interface, was also used to quantify the diffusion (see Fig. 5). In these experiments, the dangling OD signal was initially zero when the D_2O layer was capped with H_2O [e.g., Fig. 5(a), red triangles]. As the D_2O diffusively mixed with the H_2O, the D_2O at the interface increased at early times before decreasing again at longer times. An example of the calculated concentration profiles for a D_2O layer with θ_{cap} = 5 ML at several times is shown in Fig. 5(b). Overall, the calculations reproduce the trends observed in data [Fig. 5(a), dotted lines]. However, the concentration at the interface deduced from the dangling OD signal was consistently 5%–10% lower than the calculations. In the figure, the calculated concentrations have been scaled by 0.90 for θ_{cap} = 3–20 ML and 0.95 for θ_{cap} = 1 ML. [Fig. S12 shows the results without these adjustments, and Fig. S13 shows how changing $D_{tr}(T)$ ± 30% affects the calculations.] This discrepancy could be related to the fact the dangling OD signal was very weak compared to the OD-stretch band, which resulted in a noisier signal and larger uncertainty in its normalization. However, the IR spectra also showed that there was a

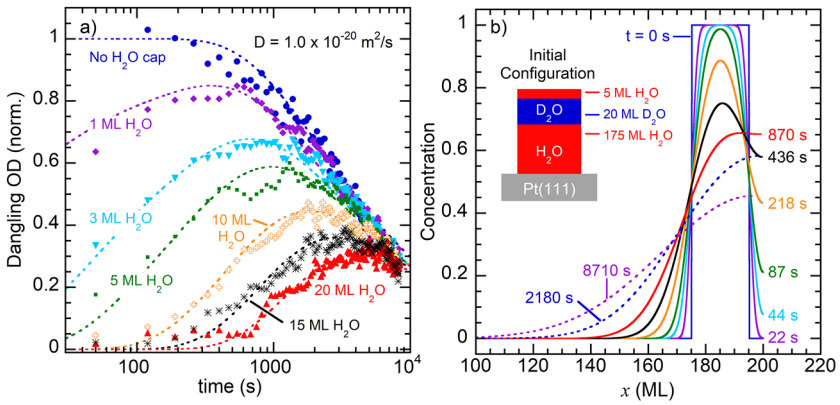

FIG. 5. (a) Normalized integrated intensity of the dangling OD peak (symbols) vs time for water films with 20 ML D_2O and 180 ML H_2O annealed at 138 K. The IR spectra were all taken at 138 K. The D_2O layers were capped with H_2O with coverages, θ_{cap}, of 0, 1, 3, 5, 10, 15, and 20 ML. The dotted lines show the calculated concentration of D_2O at the vacuum interface assuming $D_{tr} = 1.0 \times 10^{-20}$ m^2/s. (b) Calculated concentration profiles vs position (x) within the film at several times for a water film with θ_{cap} = 5 ML. The calculations, which include desorption from the film, illustrate the initial increase (solid lines) and eventual decrease (dotted lines) in the concentration of D_2O at the vacuum interface.

small amount of H/D exchange at the vacuum interface that led to the production of some isolated HOD. This effect, which was negligible for D_2O layers located in the middle of thick H_2O films, was not included in the calculation.

The red squares in Fig. 6 show the diffusion coefficients determined from measurements of the dangling OD vs $1/T$ (see also Table S2). As seen in the figure, the diffusion coefficient decreases rapidly as the temperature decreases. For the experiments shown in Fig. 3, the characteristic times, $\tau(T)$, increased exponentially as the temperature decreased (Fig. S6). As mentioned already, it is difficult to extract $D_{tr}(T)$ from those measurements. However, the experiments with D_2O layers in the middle of films with different overall thicknesses (e.g., Fig. S10) and with the D_2O layers deposited at different heights within films of the same thickness (e.g., Fig. 5) indicate that the diffusion is largely independent of the location within these water films for a wide range of film thicknesses. In that case, a single constant, λ^2, relates $\tau(T)$ to the diffusion coefficient: $D_{tr}(T) = \lambda^2/\tau(T)$. Assuming λ = 3.3 nm (see the supplementary material, Sec. S1), the black diamonds in Fig. 6 show $D_{tr}(T)$ calculated from the characteristic times. The results show that the diffusion coefficient increased by a factor of ~900 when the temperature increased from 120.2 to 144.5 K. The dashed line shows an Arrhenius fit to the data with E_a = 40.76 ± 3.5 kJ/mol and a prefactor of 2.84×10^{-5} m^2/s.

For several liquids, experiments have shown that the growth rate of a crystal in contact with its melt is proportional to the diffusion rate in the (supercooled) liquid.[55,56] The growth rate, $G(T)$, can be decomposed into kinetic and thermodynamic components.[34–36] When the thermodynamic driving force for crystallization is large, the Wilson–Frenkel model can be used to describe the growth rate: $D_{tr}(T) = \alpha G(T)/[1 - \exp(-\Delta G_{lx}(T)/k_bT)]$, where $\Delta G_{lx}(T)$ is the free energy difference between the crystal and liquid and α is a constant related to the width of the liquid/solid interface and the length of a diffusive step in the liquid. Previous work in our group measured the growth rate of crystalline ice for temperatures between 125 and 260 K.[20] It assumed that the Wilson–Frenkel model held for supercooled water and used it to extract the diffusion in the liquid. In those experiments, α was determined by comparing the measured $G(T)$ near 250 K with independent measurements of $D_{tr}(T)$ in H_2O. That value of α was then used to predict the $D_{tr}(T)$ for 125 K ≤ T ≤ 260 K. With the independent measurements of the diffusion rates presented here and those earlier growth rates, we can now test the validity of the Wilson–Frenkel model at temperatures near T_g: The blue circles in Fig. 6 show the diffusion rates previously estimated from the ice growth rates for T ≤ 152 K along with the current diffusion data. As seen in the figure, both the overall magnitude and the activation energy for $D_{tr}(T)$ predicted by the Wilson–Frenkel model are comparable to those measured here.

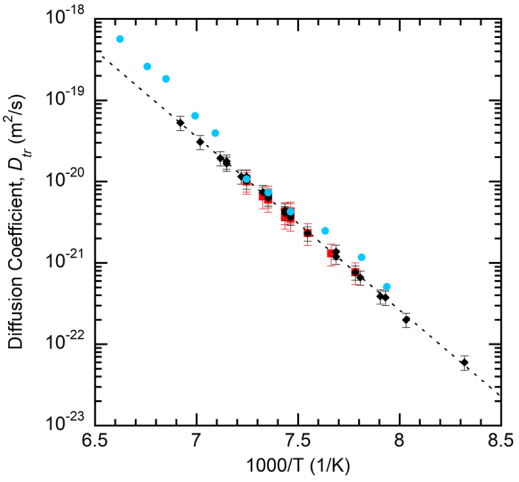

FIG. 6. Self-diffusion coefficient for low-density water, $D_{tr}(T)$, vs 1000/T. The red squares show the diffusion coefficient determined from measurements of the dangling OD signal vs annealing time (see Figs. 4 and 5). The black diamonds show $D_{tr}(T)$ determined from the characteristic diffusion times, τ, for films with 20 ML D_2O embedded within 180 H_2O (see Fig. S6). The blue circles show previous estimates of $D_{tr}(T)$ using measurements of the crystalline ice growth rate and the Wilson–Frenkel model.[20]

IV. DISCUSSION

In many supercooled liquids, the structural relaxation times, $\tau_\alpha(T)$, and viscosity, $\eta(T)$, increase very rapidly near T_g, without substantial changes in the structure.[57,58] Liquids with this property are called "fragile," and it is generally believed that the fragility is related to the development of dynamic heterogeneity within the supercooled liquids.[57–59] In contrast to fragile liquids, "strong" liquids exhibit Arrhenius temperature dependence in their dynamic properties near T_g. As the temperature is lowered, the dynamics of fragile liquids typically changes from super-Arrhenius to Arrhenius behavior, and the origin of this "fragile to strong" (FTS) transition has been extensively debated.[16,57–61] Measurements of $\tau_\alpha(T)$, $\eta(T)$, and $D_{tr}(T)$ for bulk water at 0.1 MPa and temperatures between ~235 and 373 K indicate that it is a fragile liquid.[62–65] However, two-state models of water suggest that at 0.1 MPa, it is predominantly HDL-like or LDL-like at high and low temperatures (respectively), while at intermediate temperature, it is a mixture of the two.[7,14–16] Because there is no discontinuity at low pressures,[20–23,66] thermodynamic arguments suggest that the entropy of water near T_g can only be slightly larger than for crystalline ice.[17,19,67] Using the Adam–Gibbs equation, this led to the prediction that $\eta(T)$ and $D_{tr}(T)$ should have approximately Arrhenius temperature-dependence at high and low temperatures with a gradual transition at intermediate temperatures.[17,19,67] The picture that emerges is that water's dynamical properties are characteristic of a strong liquid when it is predominately composed of one of the structural motifs, while both motifs influence its properties at intermediate temperatures.[68,69] The Arrhenius temperature dependence for $D_{tr}(T)$ reported here (see Fig. 6) is consistent with this picture.

The current results demonstrate that molecular translational diffusion on the scale of a few nanometers occurs in water for 120–144 K. The range of diffusion coefficients reported previously for these temperatures spans a wide range from none observed (or inferred) to, for example, ~10^{-16} m^2/s at 135 K.[12,13,20,28,70,71] Two experiments have reported diffusion coefficients that are a factor of 10^3 (or more) larger than those shown in Fig. 6. One, which used x-ray photon-correlation spectroscopy (XPCS) to investigate the diffusive dynamics associated with the high-to-low density transition in amorphous ice at ambient pressure, reported a diffusion coefficient of ~5×10^{-18} m^2/s at 130 K in LDL.[70] However, later results indicated that the observed diffusive dynamics were associated with the

motion of nanometer scale domains within the liquids, not molecular diffusion.[72] Another experiment trapped CO_2 in ASW as the films were grown at 80–100 K and then obtained the tracer diffusion coefficient to the diffusion of water.[71] The reported diffusion coefficients (e.g., 8.6×10^{-17} m^2/s at 135 K) are difficult to reconcile with the observations. The typical distance a molecule diffuses during a time, t, is $x_{diff} \sim \sqrt{6D_{tr}t}$ (in 3 dimensions). T_g is often taken to be the temperature at which the structural relaxation time for a liquid is ~100 s. Assuming that $D_{tr} = 8.6 \times 10^{-17}$ m^2/s at 135 K and $t = 100$ s, one finds that $x_{diff} \sim 230$ nm—a distance that heuristically seems to be far larger than needed for equilibration. In contrast, we find that $D_{tr} = 6.25 \times 10^{-21}$ m^2/s at 136 K, which gives $x_{diff} \sim 2$ nm for $t = 100$ s. Note that if the diffusion coefficient was 8.6×10^{-17} m^2/s at 135 K in our experiments, then a film with 20 ML of D_2O in the middle of a film with a total coverage of 200 ML would mix on a characteristic timescale of ~0.2 s, instead of the ~2000 s that was observed (see Table S1).

In their H/D exchange experiments, Fisher and Devlin argued that molecular rotations could account for their results, while diffusion could not.[12] As mentioned in the Introduction, Johari already discussed how diffusion might account for their observations.[25] We note that Fisher and Devlin's results do not rule out diffusion—instead they imply that rotations created isolated HOD on a timescale that was short compared to diffusion. Because the relative rates of translational and rotational diffusion in water are unknown for the temperatures of those experiments (between 115 and 122 K), whether or not faster rotations accounts for Fisher and Devlin's results remains an open question. Understanding the effects of rotations vs translations is probably also germane for explaining the intriguing isotope effects observed in the glass transition temperatures for LDA, HDA, and ice VI.[13] However, the observed correlations among the glass transition temperatures do not exclude the possibility of translational diffusion in LDA.

H/D isotope effects influence the structure and dynamics of water.[73] For example, the temperature of maximum density at ambient pressure for D_2O is 7.2 K higher than it is for H_2O. In addition, diffusion is faster, and viscosity is lower in H_2O compared to D_2O in normal and moderately supercooled water (e.g., 245–300 K). Early work, which suggested a possible singularity in the H_2O's properties at ~228 K, found a similar behavior in D_2O with an apparent singularity at ~233 K.[24] Isotope effects are also notable in amorphous ices at cryogenic temperatures (e.g., the ~4 K shift in T_g between D_2O and H_2O discussed above).[13,74] Furthermore, the dielectric relaxation times in D_2O are shifted by up to 12 K near T_g.[75] While most of experiments on isotope effects have focused on pure H_2O and D_2O, experiments using isotopic mixtures typically show that the property of interest (e.g., density or viscosity) varies smoothly between the 2 pure end points as the composition is changed.[76–78] Because the experiments reported here involve mixtures of H_2O and D_2O, it is likely that the diffusion coefficients shown in Fig. 6 are smaller (larger) than the coefficients for pure H_2O (D_2O). However, the magnitude of the isotope effect on diffusion at these low temperatures remains to be determined.

Some previous experiments have reported diffusion coefficients that are comparable to those found here, but with larger activation energies (see Fig. S14). Brown and George,[28] who used laser-induced thermal desorption (LITD) to monitor diffusive mixing in layer $H_2{}^{18}O$ and $H_2{}^{16}O$ films for 155 K ≤ T ≤ 165 K, found $D_{tr} = 1.5(\pm0.5) \times 10^{-19}$ m^2/s at 160 K with $E_a = 69.9$ kJ/mol. Our group also investigated mixing in isotopically layer water films in early reports and found an even larger activation energy (~170 kJ/mol for ~147 K < T < 157 K).[29,30] However, as noted in the Introduction, subsequent research showed that the observed mixing was coupled to crystallization in those experiments such that the diffusion could not be determined with that approach.[31,32] We believe it is likely that crystallization also affected the experiments of Brown and George, which were conducted at even higher temperatures. To address the limitations in those earlier experiments, some of us (RSS, BDK, and GAK) have recently revisited the diffusion in supercooled water by monitoring water desorption from layered films of $H_2{}^{16}O$ and $H_2{}^{18}O$.[79] Those new experiments used very low heating rates to decouple the diffusive mixing from the crystallization. Overall, the agreement between the two sets of experiments is quite good (see Fig. S14), and the reported activation energies agree within the uncertainties (40.8 ± 3.5 and 36.0 ± 4 kJ/mol). The minor differences between the two experiments are consistent with the expectations based on the isotope effects discussed above. Because isotope effects are typically smaller in $H_2{}^{18}O$ and $H_2{}^{16}O$ compared to those in H_2O and D_2O, those experiments should more closely reflect the diffusion coefficient in ordinary water.

V. CONCLUSIONS

The experiments reported here used IR spectroscopy to track the motion of intact D_2O molecules within majority of H_2O films with coverages up to 300 ML, which corresponded to film thicknesses of up to ~100 nm. Isotopically layered films of D_2O and H_2O were grown on a Pt(111) surface at 108 K—a temperature at which diffusion was negligible—and subsequently annealed at temperatures from 120 to 144 K. The experiments were conducted under conditions where H/D exchange was minimized such that the results were insensitive to the rotational diffusion of the water molecules. In particular, if there was only rotational diffusion and no translational diffusion, the IR spectra would not have changed as the films were annealed. Instead, the results demonstrate that the initial, non-uniform distribution of D_2O and H_2O within the water films evolved toward a uniform distribution through translational diffusion of the intact water molecules. For experiments with the D_2O probe layers initially sandwiched between 2 H_2O layers, the rate of diffusive mixing was independent of the total thickness, x_{film}, for (at least) $x_{film} > 20$ nm. For films with a total coverage of 200 ML, any variations of the diffusion coefficient vs the distance from the vacuum interface were below the uncertainty of the measurements (i.e., <±30%). The translational diffusion coefficient had an Arrhenius temperature dependence with an activation energy of 40.8 ± 3.5 kJ/mol showing that water is strong liquid at and near the calorimetric glass transition at 136 K. The results also indicate that LDA, ASW, and HGW all relax to the same supercooled liquid water state upon sufficient annealing at and near T_g.

SUPPLEMENTARY MATERIAL

The supplementary material includes figures showing various IR spectra in support of discussion points in the main article (Figs. S1–S4 and S10). Figures S5 and S11 show the IR integrals vs time for all the experiments used to determine the diffusion

coefficients shown in Fig. 6. Those figures also show the effect of increasing or decreasing the estimates of the characteristic times by ±20% (Fig. S5) or ±30% (Fig. S11) on the analysis. The characteristic times (see Fig. S6) and diffusion coefficients are also given in Tables S1 and S2. Figures S12 and S13 provide additional information for the results shown in Fig. 5. Figure S7 shows IR integrals vs time for 200 ML water films with a 5 ML D_2O layer in the middle, and Fig. S8 shows the same data in Fig. 3 but with a linear time axis. Figure S9 shows examples of eventual crystallization in the annealed films. Finally, Fig. S14 shows a comparison of the diffusion coefficients in the current work to previous experiments.

ACKNOWLEDGMENTS

This work was supported by the U.S. Department of Energy (DOE), Office of Science, Office of Basic Energy Sciences, Division of Chemical Sciences, Geosciences, and Biosciences, Condensed Phase and Interfacial Molecular Science program, FWP Grant No. 16248.

AUTHOR DECLARATIONS

Conflict of Interest

The authors have no conflicts to disclose.

Author Contributions

The work was conceptualized by G.A.K. and B.D.K. G.A.K. and M.K.D. performed the experiments and analyzed the data. K.G. performed preliminary experiments. All authors contributed ideas to refine the experiments. G.A.K. wrote the paper with input from all the authors.

Greg A. Kimmel: Conceptualization (equal); Formal analysis (lead); Funding acquisition (equal); Investigation (lead); Methodology (equal); Project administration (equal); Resources (equal); Supervision (equal); Writing – original draft (lead); Writing – review & editing (equal). **Megan K. Dunlap**: Formal analysis (supporting); Investigation (supporting); Methodology (supporting); Writing – review & editing (equal). **Kirill Gurdumov**: Conceptualization (supporting); Formal analysis (supporting); Investigation (supporting); Methodology (supporting); Project administration (equal); Resources (equal); Supervision (equal); Writing – review & editing (supporting). **R. Scott Smith**: Conceptualization (supporting); Formal analysis (supporting); Funding acquisition (equal); Investigation (supporting); Methodology (supporting); Project administration (equal); Resources (equal); Supervision (equal); Writing – review & editing (supporting). **Loni Kringle**: Funding acquisition (supporting); Investigation (supporting); Methodology (supporting); Resources (supporting); Writing – review & editing (supporting). **Bruce D. Kay**: Conceptualization (equal); Formal analysis (supporting); Funding acquisition (equal); Methodology (equal); Project administration (equal); Resources (equal); Supervision (equal); Writing – review & editing (equal).

DATA AVAILABILITY

The data that support the findings of this study are available within the article and its supplementary material.

REFERENCES

[1] E. F. Burton and W. F. Oliver, "X-ray diffraction patterns of ice," Nature **135**, 505–506 (1935).
[2] E. Mayer, "New method for vitrifying water and other liquids by rapid cooling of their aerosols," J. Appl. Phys. **58**, 663–667 (1985).
[3] O. Mishima, L. D. Calvert, and E. Whalley, "'Melting ice' I at 77 K and 10 kbar: A new method of making amorphous solids," Nature **310**, 393–395 (1984).
[4] O. Mishima, L. D. Calvert, and E. Whalley, "An apparently first-order transition between two amorphous phases of ice induced by pressure," Nature **314**, 76–78 (1985).
[5] T. Loerting, C. Salzmann, I. Kohl, E. Mayer, and A. Hallbrucker, "A second distinct structural 'state' of high-density amorphous ice at 77 K and 1 bar," Phys. Chem. Chem. Phys. **3**, 5355–5357 (2001).
[6] A. Rosu-Finsen, M. B. Davies, A. Amon, H. Wu, A. Sella, A. Michaelides, and C. G. Salzmann, "Medium-density amorphous ice," Science **379**, 474–478 (2023).
[7] O. Mishima and H. E. Stanley, "The relationship between liquid, supercooled and glassy water," Nature **396**, 329–335 (1998).
[8] C. A. Angell, "Insights into phases of liquid water from study of its unusual glass-forming properties," Science **319**, 582–587 (2008).
[9] K. Amann-Winkel, R. Böhmer, F. Fujara, C. Gainaru, B. Geil, and T. Loerting, "Colloquium: Water's controversial glass transitions," Rev. Mod. Phys. **88**, 011002 (2016).
[10] A. Hallbrucker, E. Mayer, and G. P. Johari, "Glass-liquid transition and the enthalpy of devitrification of annealed vapor-deposited amorphous solid water: A comparison with hyperquenched glassy water," J. Phys. Chem. **93**, 4986–4990 (1989).
[11] A. Hallbrucker, E. Mayer, and G. P. Johari, "The heat capacity and glass transition of hyperquenched glassy water," Philos. Mag. B **60**, 179–187 (1989).
[12] M. Fisher and J. P. Devlin, "Defect activity in amorphous ice from isotopic exchange data: Insight into the glass transition," J. Phys. Chem. **99**, 11584–11590 (1995).
[13] J. J. Shephard and C. G. Salzmann, "Molecular reorientation dynamics govern the glass transitions of the amorphous ices," J. Phys. Chem. Lett. **7**, 2281–2285 (2016).
[14] P. G. Debenedetti, "Supercooled and glassy water," J. Phys.: Condens. Matter **15**, R1669–R1726 (2003).
[15] H. Tanaka, "Bond orientational order in liquids: Towards a unified description of water-like anomalies, liquid-liquid transition, glass transition, and crystallization," Eur. Phys. J. E **35**, 113 (2012).
[16] P. Gallo, K. Amann-Winkel, C. A. Angell, M. A. Anisimov, F. Caupin, C. Chakravarty, E. Lascaris, T. Loerting, A. Z. Panagiotopoulos, J. Russo, J. A. Sellberg, H. E. Stanley, H. Tanaka, C. Vega, L. Xu, and L. G. M. Pettersson, "Water: A tale of two liquids," Chem. Rev. **116**, 7463–7500 (2016).
[17] F. W. Starr, C. A. Angell, and H. E. Stanley, "Prediction of entropy and dynamic properties of water below the homogeneous nucleation temperature," Physica A **323**, 51–66 (2003).
[18] H. Tanaka, "Two-order-parameter description of liquids: Critical phenomena and phase separation of supercooled liquids," J. Phys.: Condens. Matter **11**, L159–L168 (1999).
[19] F. Caupin, "Predictions for the properties of water below its homogeneous crystallization temperature revisited," J. Non-Cryst. Solids: X **14**, 100090 (2022).
[20] Y. Xu, N. G. Petrik, R. S. Smith, B. D. Kay, and G. A. Kimmel, "Growth rate of crystalline ice and the diffusivity of supercooled water from 126 to 262 K," Proc. Natl. Acad. Sci. U. S. A. **113**, 14921–14925 (2016).
[21] K. H. Kim, A. Späh, H. Pathak, F. Perakis, D. Mariedahl, K. Amann-Winkel, J. A. Sellberg, J. H. Lee, S. Kim, J. Park, K. H. Nam, T. Katayama, and A. Nilsson, "Maxima in the thermodynamic response and correlation functions of deeply supercooled water," Science **358**, 1589–1593 (2017).
[22] L. Kringle, W. A. Thornley, B. D. Kay, and G. A. Kimmel, "Reversible structural transformations in supercooled liquid water from 135 to 245 K," Science **369**, 1490–1492 (2020).
[23] C. R. Krüger, N. J. Mowry, G. Bongiovanni, M. Drabbels, and U. J. Lorenz, "Electron diffraction of deeply supercooled water in no man's land," Nat. Commun. **14**, 2812 (2023).
[24] C. A. Angell, "Supercooled water," Annu. Rev. Phys. Chem. **34**, 593–630 (1983).

[25]G. P. Johari, "Amorphous solid water's isotopic exchange kinetics," J. Chem. Phys. **117**, 2782–2789 (2002).
[26]J. H. Melillo, D. Cangialosi, V. Di Lisio, E. Steinrücken, M. Vogel, and S. Cerveny, "Complexity of confined water vitrification and its glass transition temperature," Proc. Natl. Acad. Sci. U. S. A. **121**, e2407030121 (2024).
[27]R. S. Smith, N. G. Petrik, G. A. Kimmel, and B. D. Kay, "Thermal and nonthermal physiochemical processes in nanoscale films of amorphous solid water," Acc. Chem. Res. **45**, 33–42 (2012).
[28]D. E. Brown and S. M. George, "Surface and bulk diffusion of $H_2{}^{18}O$ on single-crystal $H_2{}^{16}O$ ice multilayers," J. Phys. Chem. **100**, 15460–15469 (1996).
[29]R. S. Smith and B. D. Kay, "The existence of supercooled liquid water at 150 K," Nature **398**, 788–791 (1999).
[30]R. S. Smith, Z. Dohnálek, G. A. Kimmel, K. P. Stevenson, and B. D. Kay, "The self-diffusivity of amorphous solid water near 150 K," Chem. Phys. **258**, 291–305 (2000).
[31]S. M. McClure, E. T. Barlow, M. C. Akin, D. J. Safarik, T. M. Truskett, and C. B. Mullins, "Transport in amorphous solid water films: Implications for self-diffusivity," J. Phys. Chem. B **110**, 17987–17997 (2006).
[32]S. M. McClure, D. J. Safarik, T. M. Truskett, and C. B. Mullins, "Evidence that amorphous water below 160 K is not a fragile liquid," J. Phys. Chem. B **110**, 11033–11036 (2006).
[33]R. S. Smith, N. G. Petrik, G. A. Kimmel, and B. D. Kay, "Communication: Proton exchange in low temperature co-mixed amorphous H_2O and D_2O films: The effect of the underlying Pt(111) and graphene substrates," J. Chem. Phys. **149**, 081104 (2018).
[34]J. W. Cahn, W. B. Hillig, and G. W. Sears, "The molecular mechanism of solidification," Acta Metall. **12**, 1421–1439 (1964).
[35]J. Q. Broughton, G. H. Gilmer, and K. A. Jackson, "Crystallization rates of a Lennard-Jones liquid," Phys. Rev. Lett. **49**, 1496–1500 (1982).
[36]M. L. F. Nascimento and E. Dutra Zanotto, "Does viscosity describe the kinetic barrier for crystal growth from the liquidus to the glass transition?," J. Chem. Phys. **133**, 174701 (2010).
[37]M. K. Dunlap, L. Kringle, B. D. Kay, and G. A. Kimmel, "Proton diffusion and hydrogen/deuterium exchange in amorphous solid water at temperatures from 114 to 134 K," J. Chem. Phys. **161**, 244504 (2024).
[38]G. A. Kimmel, K. P. Stevenson, Z. Dohnálek, R. S. Smith, and B. D. Kay, "Control of amorphous solid water morphology using molecular beams. I. Experimental results," J. Chem. Phys. **114**, 5284–5294 (2001).
[39]K. P. Stevenson, G. A. Kimmel, Z. Dohnálek, R. S. Smith, and B. D. Kay, "Controlling the morphology of amorphous solid water," Science **283**, 1505–1507 (1999).
[40]S. Nie, P. J. Feibelman, N. C. Bartelt, and K. Thürmer, "Pentagons and heptagons in the first water layer on Pt(111)," Phys. Rev. Lett. **105**, 026102 (2010).
[41]T. Loerting, M. Bauer, I. Kohl, K. Watschinger, K. Winkel, and E. Mayer, "Cryoflotation: Densities of amorphous and crystalline ices," J. Phys. Chem. B **115**, 14167–14175 (2011).
[42]C. Yuan, R. S. Smith, and B. D. Kay, "Surface and bulk crystallization of amorphous solid water films: Confirmation of 'top-down' crystallization," Surf. Sci. **652**, 350–354 (2016).
[43]M. D. Ediger, "Perspective: Highly stable vapor-deposited glasses," J. Chem. Phys. **147**, 210901 (2017).
[44]S. F. Swallen, K. L. Kearns, M. K. Mapes, Y. S. Kim, R. J. McMahon, M. D. Ediger, T. Wu, L. Yu, and S. Satija, "Organic glasses with exceptional thermodynamic and kinetic stability," Science **315**, 353–356 (2007).
[45]L. Kringle, W. A. Thornley, B. D. Kay, and G. A. Kimmel, "Structural relaxation and crystallization in supercooled water from 170 to 260 K," Proc. Natl. Acad. Sci. U. S. A. **118**, e2022884118 (2021).
[46]D. Williams, "Frequency assignments in infra-red spectrum of water," Nature **210**, 194–195 (1966).
[47]A. B. McCoy, "The role of electrical anharmonicity in the association band in the water spectrum," J. Phys. Chem. B **118**, 8286–8294 (2014).
[48]H. J. Bakker and J. L. Skinner, "Vibrational spectroscopy as a probe of structure and dynamics in liquid water," Chem. Rev. **110**, 1498–1517 (2010).
[49]G. Ritzhaupt and J. P. Devlin, "Infrared-spectrum of D_2O vibrationally decoupled in glassy H_2O," J. Chem. Phys. **67**, 4779–4780 (1977).
[50]G. Cicero, J. C. Grossman, E. Schwegler, F. Gygi, and G. Galli, "Water confined in nanotubes and between graphene sheets: A first principle study," J. Am. Chem. Soc. **130**, 1871–1878 (2008).
[51]D. T. Limmer, A. P. Willard, P. Madden, and D. Chandler, "Hydration of metal surfaces can be dynamically heterogeneous and hydrophobic," Proc. Natl. Acad. Sci. U. S. A. **110**, 4200–4205 (2013).
[52]A. P. Willard and D. Chandler, "The molecular structure of the interface between water and a hydrophobic substrate is liquid-vapor like," J. Chem. Phys. **141**, 18c519 (2014).
[53]B. Rowland and J. P. Devlin, "Spectra of dangling OH groups at ice cluster surfaces and within pores of amorphous ice," J. Chem. Phys. **94**, 812–813 (1991).
[54]V. Buch and J. P. Devlin, "Spectra of dangling OH bonds in amorphous ice: Assignment to 2- and 3-coordinated surface molecules," J. Chem. Phys. **94**, 4091–4092 (1991).
[55]M. K. Mapes, S. F. Swallen, and M. D. Ediger, "Self-diffusion of supercooled *o*-terphenyl near the glass transition temperature," J. Phys. Chem. B **110**, 507–511 (2006).
[56]K. L. Ngai, J. H. Magill, and D. J. Plazek, "Flow, diffusion and crystallization of supercooled liquids: Revisited," J. Chem. Phys. **112**, 1887–1892 (2000).
[57]L. Berthier and G. Biroli, "Theoretical perspective on the glass transition and amorphous materials," Rev. Mod. Phys. **83**, 587–645 (2011).
[58]M. D. Ediger, "Spatially heterogeneous dynamics in supercooled liquids," Annu. Rev. Phys. Chem. **51**, 99–128 (2000).
[59]F. Mallamace, C. Branca, C. Corsaro, N. Leone, J. Spooren, S. H. Chen, and H. E. Stanley, "Transport properties of glass-forming liquids suggest that dynamic crossover temperature is as important as the glass transition temperature," Proc. Natl. Acad. Sci. U. S. A. **107**, 22457–22462 (2010).
[60]Y. S. Elmatad, D. Chandler, and J. P. Garrahan, "Corresponding states of structural glass formers," J. Phys. Chem. B **113**, 5563–5567 (2009).
[61]M. De Marzio, G. Camisasca, M. Rovere, and P. Gallo, "Fragile to strong crossover and widom line in supercooled water: A comparative study," Front. Phys. **13**, 136103 (2018).
[62]K. Ito, C. T. Moynihan, and C. A. Angell, "Thermodynamic determination of fragility in liquids and a fragile-to-strong liquid transition in water," Nature **398**, 492–495 (1999).
[63]W. S. Price, H. Ide, and Y. Arata, "Self-diffusion of supercooled water to 238 K using PGSE NMR diffusion measurements," J. Phys. Chem. A **103**, 448–450 (1999).
[64]A. Dehaoui, B. Issenmann, and F. Caupin, "Viscosity of deeply supercooled water and its coupling to molecular diffusion," Proc. Natl. Acad. Sci. U. S. A. **112**, 12020–12025 (2015).
[65]L. P. Singh, B. Issenmann, and F. Caupin, "Pressure dependence of viscosity in supercooled water and a unified approach for thermodynamic and dynamic anomalies of water," Proc. Natl. Acad. Sci. U. S. A. **114**, 4312–4317 (2017).
[66]L. Kringle, B. D. Kay, and G. A. Kimmel, "Structural relaxation of water during rapid cooling from ambient temperatures," J. Chem. Phys. **159**, 064509 (2023).
[67]C. A. Angell, C. T. Moynihan, and M. Hemmati, "'Strong' and 'superstrong' liquids, and an approach to the perfect glass state via phase transition," J. Non-Cryst. Solids **274**, 319–331 (2000).
[68]N. J. Hestand and J. L. Skinner, "Perspective: Crossing the Widom line in no man's land: Experiments, simulations, and the location of the liquid-liquid critical point in supercooled water," J. Chem. Phys. **149**, 140901 (2018).
[69]R. Shi, J. Russo, and H. Tanaka, "Origin of the emergent fragile-to-strong transition in supercooled water," Proc. Natl. Acad. Sci. U. S. A. **115**, 9444–9449 (2018).
[70]F. Perakis, K. Amann-Winkel, F. Lehmkühler, M. Sprung, D. Mariedahl, J. A. Sellberg, H. Pathak, A. Späh, F. Cavalca, D. Schlesinger, A. Ricci, A. Jain, B. Massani, F. Aubree, C. J. Benmore, T. Loerting, G. Grübel, L. G. M. Pettersson, and A. Nilsson, "Diffusive dynamics during the high-to-low density transition in amorphous ice," Proc. Natl. Acad. Sci. U. S. A. **114**, 8193–8198 (2017).
[71]P. Ghesquière, T. Mineva, D. Talbi, P. Theulé, J. A. Noble, and T. Chiavassa, "Diffusion of molecules in the bulk of a low density amorphous ice from molecular dynamics simulations," Phys. Chem. Chem. Phys. **17**, 11455–11468 (2015).
[72]H. Li, M. Ladd-Parada, A. Karina, F. Dallari, M. Reiser, F. Perakis, N. N. Striker, M. Sprung, F. Westermeier, G. Grübel, W. Steffen, F. Lehmkühler, and K.

Amann-Winkel, "Intrinsic dynamics of amorphous ice revealed by a heterodyne signal in X-ray photon correlation spectroscopy experiments," J. Phys. Chem. Lett. **14**, 10999–11007 (2023).
[73]M. Ceriotti, W. Fang, P. G. Kusalik, R. H. McKenzie, A. Michaelides, M. A. Morales, and T. E. Markland, "Nuclear quantum effects in water and aqueous systems: Experiment, theory, and current challenges," Chem. Rev. **116**, 7529–7550 (2016).
[74]G. P. Johari, A. Hallbrucker, and E. Mayer, "Isotope and impurity effects on the glass transition and crystallization of pressure-amorphized hexagonal and cubic ice," J. Chem. Phys. **95**, 6849–6855 (1991).
[75]C. Gainaru, A. L. Agapov, V. Fuentes-Landete, K. Amann-Winkel, H. Nelson, K. W. Köster, A. I. Kolesnikov, V. N. Novikov, R. Richert, R. Böhmer, T. Loerting, and A. P. Sokolov, "Anomalously large isotope effect in the glass transition of water," Proc. Natl. Acad. Sci. U. S. A. **111**, 17402–17407 (2014).
[76]E. Swift, "The temperature of maximum density of D_2O and of its mixtures with H_2O," J. Am. Chem. Soc. **61**, 1293–1294 (1939).
[77]U. Kaatze, "Dielectric-relaxation of H_2O/D_2O mixtures," Chem. Phys. Lett. **203**, 1–4 (1993).
[78]O. Gajst, R. Simkovitch, and D. Huppert, "Anomalous H^+ and D^+ excited-state proton-transfer rate in H_2O/D_2O mixtures," J. Phys. Chem. A **121**, 6917–6924 (2017).
[79]R. S. Smith, W. A. Thornley, G. A. Kimmel, and B. D. Kay, "Supercooled liquid water diffusivity at temperatures near the glass transition temperature," J. Phys. Chem. Lett. **16**, 3198–3205 (2025).